Journal of Thermal Analysis and Calorimetry (2019) 137:501–511
https://doi.org/10.1007/s10973-018-7955-7

Semi-analytical modeling of non-premixed counterflow combustion of metal dust

Seyed Amir Hossein Madani[1] · Mehdi Bidabadi[1] · Nafiseh Mohammadian Aftah[2] · Abolfazl Afzalabadi[1]

Received: 9 April 2018 / Accepted: 24 November 2018 / Published online: 7 December 2018

Abstract

In this study, a semi-analytical model is developed for non-premixed combustion of metal dusts in counterflow configuration. Combustion domain is divided into three separate zones, each of which possesses corresponding mass and energy conservation equations as well as boundary and jump conditions. Metal dust, assumed to be aluminum, undergoes an Arrhenius-type reaction with oxidizer, when it is heated enough to reach the ignition temperature. Dimensionless forms of conservation equations are derived and utilized to elucidate the combustion characteristics. The effects of oxidizer Lewis number and fuel mass concentration on the flame position and temperature are discussed thoroughly. In addition, temperature distribution of the whole domain is calculated by numerically solving the system of partial differential equations. In order to track particles through combustion domain, Lagrangian equations of motion are solved either mathematically or numerically, considering thermophoretic, weight, buoyancy and drag forces. The effects of thermophoretic force on the particle path are investigated, and the deviation of particle from carrier neutral gas direction is obtained. The results showed a great agreement with the data reported in the literature highlighting the fact that the presented model is an efficient one to accurately model the non-premixed counterflow combustion of metal dust.

Keywords Non-premixed combustion · Aluminum dust cloud · Mathematical modeling · Counterflow configuration · Thermophoresis effect · Particle tracking

List of symbols

a	Strain rate (s^{-1})
C_a	Gas heat capacity (J kg^{-1} K^{-1})
C_D	Drag coefficient
C_p	Particle heat capacity (J kg^{-1} K^{-1})
$\bar{C}$	Mean thermal velocity of gaseous molecules (m s^{-1})
D_O	Oxidizer diffusion coefficient (m^2 s^{-1})
d_p	Particle diameter (m)
D_T	Thermal diffusion coefficient (m^2 s^{-1})
E_a	Activation energy (J)
F_B	Buoyancy force (N)
F_D	Drag force (N)
F_G	Gravity force (N)
F_T	Thermophoretic force (N)
Kn	Knudsen number
Le	Lewis number
m_p	Particle mass (kg)
n_p	Number of particles per unit volume (m^{-3})
Q	Heat released per unit mass of fuel (J kg^{-1})
R	Universal gas constant (J mol^{-1} K^{-1})
T	Temperature (K)
T_a	Dimensionless activation energy
u	Velocity in x-direction (m s^{-1})
U	Particle velocity (m s^{-1})
v	Velocity in y-direction (m s^{-1})
V_b	Burning velocity (m s^{-1})
W_F	Molecular weight of fuel (kg mol^{-1})
x_f	Initiation point of flame
Y_O	Oxidizer mass fraction
Y_s	Solid fuel mass fraction
$Y_{s-\infty}$	Primary mass fraction of solid fuel

Greek symbols

μ	Viscosity (Pa s)
λ	Particle mean free path (m)

✉ Seyed Amir Hossein Madani
amiroseinmadani@gmail.com

[1] School of Mechanical Engineering, Iran University of Science and Technology (IUST), Narmak, Tehran 16846-13114, Iran

[2] Faculty of New Sciences and Technologies, University of Tehran, North Kargar St., Amir Abad, Tehran, Iran

θ Dimensionless temperature
ϑ Stoichiometric mass ratio
ρ Density (kg m^{-3})

Subscripts

o Oxidizer
s Solid fuel
ig Ignition
p Particle

Introduction

Metal particles have been drawn a great deal of attention from scientist over the years and are now extensively utilized in various fields such as bioengineering [1], consumer electronics [2], thermal and chemical processes [3–8], catalysis [9, 10], and, most importantly, renewable energies [11, 12]. Recently, with the development of industrial processes and population growth, human need for energy have become more of an enormous challenge regarding the deficiency of the fossil fuels in near future. Besides, the increasing global warming emissions have made scientists to devise novel solutions to substitute the existing pollutant fuels. Therefore, it is now a great concern to introduce and utilize effective renewable energy sources including alternative fuels such as metal particles. Employing metal powders as fuel has its own pros and cons like every other renewable source; however, its advantages such as abundancy, zero produced carbon and the ability to collect and recover the by-products of metal combustion overcome the complexity and uncertainty of methods that can efficiently use these kinds of fuels [13]. On the other hand, the industries working with small particles are always exposed to the risk of explosion, if the particles are finely dispersed in the medium. Reaching a certain mass concentration required for ignition and being triggered by any energy source, the flame kernel develops and propagates very fast through the medium, which in most cases results in substantial financial loss and casualties [14–16]. Therefore, implementing novel clean energy technologies and safety issues highlights the importance of particle combustion analysis. Although researchers have been working on different aspects of the field for six decades, theoretical and experimental researches have not comprehensively been focused on a robust approach to extract metal dust energy. This is due to problems that arise when working in this area, such as difficulty in achieving the stable laboratory conditions, eliminating the gravity effects on experiments, the unknown nature of the combustion of metals, and the presence of numerous parameters affecting the combustion characteristics.

The particles burning mechanism can be classified according to their type, size and volatility. The volatile particles first evaporate, and the resulting gases take part in a homogenous reaction with the oxidizer, while nonvolatile particles combustion is heterogeneous. Metal particles combustion is mostly modeled as heterogeneous, and the so-called surface reaction happens at the interface of the particle and oxidizer [17]. In the present paper, aluminum particles are considered to be nonvolatile particles attending the irreversible reaction that follows the Arrhenius law [18] and occurs at the interface of fuel and oxidizer. Aluminum particles are chosen as fuel component due to availability, high heat release per mass (second among metals) [19], non-toxic by-products and stability.

Dust particle combustion is generally studied by many researchers for a wide variety of configurations and in diverse combustion systems. For example, flame propagation through dispersed aluminum particles is broadly studied by many researchers. A general relation for burning time of a single aluminum particle is presented by Beckstead [20]. He cataloged more than 400 data points from ten different sources and used various proposed models with pivotal environmental parameters to achieve a more realistic combustion model. The correlation considers the effect of different reactants such as CO_2, water vapor and air and has been widely adopted since. Goroshin et al. [21] reported the burning velocities of fuel-rich aluminum mixtures in a Bunsen-type burner. Based on the results, mixture burning rate is more influenced by oxygen concentration rather than dust concentration. It was also found that the carrier neutral gas plays a significant role in the burning velocity. Trunov et al. [22] reviewed the existing models predicting the combustion characteristics of aluminum dust and acclaimed that the models fail to investigate the effect of particle diameter changes and experimental conditions on combustion characteristics. A logical explanation was also presented for the relation between processes governing ignition and oxidation of aluminum powders. Risha et al. [23] experimentally investigated the laminar flame speed of aluminum fuel blends with different particle sizes and mixture compositions. While it may be partly responsible for temperature distribution change, the dust concentration was found to have low effect in flame speed. The impact of oxidizer stream speed was explored to determine the dependence of flame speed on jet momentum, and it was found that flame speed increases with the increase in oxidizer shear velocity until it reaches a constant rate. In another study, Huang et al. [24] numerically investigated the combustion of aluminum dust for a wide range of sizes. Their proposed model succeeded to predict the effects of particles size, equivalence ratio and chemical kinetics on the flame speed and temperature distribution. They acclaimed that no

universal law exists to be applied for the entire range of sizes. Our research group mathematically modeled the flame propagation of solid dust and presented the relevant dynamic parameters of the flame. A one-dimensional model for abrupt combustion of aluminum was developed by Bidabadi et al. [25]. The model calculated the propagation speed, minimum ignition energy and quenching distance for uniformly dispersed particles which have low burning time (Al + Mg) in a quiescent reaction medium. The model was also applied to a three-dimensional distribution of particles, and the burning time was included. Later, the model was employed to investigate the combustion of randomly distributed particles [26], hybrid cloud of particles [27] and consideration of radiative heat transfer mechanism [28]. Also the dependency of flame speed and temperature on the particle concentration as well as minimum ignition energy and quenching distances was presented and discussed.

The complexity of the combustion process has prevented scientists to reach a comprehensive model, resulting in more precise and delicate methods. Combustion analysis in a counterflow configuration allows the researchers to shed more light on parameters such as flame stretch, gradual diffusion, radiation heat transfer and chemical kinetics. It is also more frequently encountered in practical combustion compared to the flame propagating systems. However, due to safety issues and difficulties in conducting the tests, less attention has been paid to the counterflow combustion, especially for solid particles. Fuel and oxidizer streams enter the combustion domain either separately which forms diffusion flames, or combined with each other, entering from two opposing nozzles. Seshadri and Tervino [29] presented an asymptotic solution for diffusion flames of lean methane–air mixtures considering relatively low activation energy. They characterized the effects of oxidizer and gaseous flame Lewis number on the flame position, flame temperature and heat loss. Gue et al. [30] numerically investigated the effects of radiation on the heat loss and extinction of counterflow premixed lean methane–air flame. They found a relation between stretch rate and radiative heat loss which causes the flame to extinct. The impacts of fuel concentration, temperature and strain rate on the extinction and auto-ignition of an *n*-heptane/air counterflow flame were investigated by Seiser et al. [31]. One major result of their research was that strain rate is a more substantial parameter than temperature when it comes to the low-temperature chemistry. Bidabadi et al. [32] used analytical approach to study the characteristics of flame in a counterflow configuration. The model was based on three different zones, and a two-phase mixture model was implemented to simulate the structure of dispersed organic particles in air. In addition, the effect of heat loss was taken into account and Lycopodium was considered as fuel. The relation between gaseous phase and fuel particles mass fraction as a function of the distance from the stagnation plane was calculated, and the effects of strain rate on flame temperature and flame velocity were obtained. In another study, burning speed, stabilization point and the effect of strain rate for the premixed combustion of aluminum dust cloud in a counterflow configuration have been analyzed [33]. Concerning thermophoresis, Bidabadi et al. [34] presented a model analyzing the effects of thermophoresis on the combustion of aluminum particles and water. To the best of our knowledge, an analytical model of the non-premixed combustion of metal dust in a counterflow configuration is presented in this paper for the first time. Furthermore, particles have been chased from the fuel nozzle to the outlet and the effect of thermophoresis is analyzed. The domain is divided into three zones including a preheat zone where the rate of chemical reaction is small, a reaction zone where the particles reach the ignition temperature and, finally, a post-flame zone where the rate of chemical reaction presumed to be small due to the lack of fuel. The paper also investigates the influence of oxidizer Lewis number and fuel mass concentration on the flame temperature and position. The results of aluminum burning rate indicate a reasonable agreement with the existing data in the literature.

Mathematical model

The present model investigates the non-premixed combustion of metal particles in a counterflow configuration using analytical and numerical approaches simultaneously. The fuel and oxidizer flows whose velocities are the same move toward the stagnation plane from the nozzles in the both sides of the domain. Particles are assumed to react with the oxidizer and burn heterogeneously. Aluminum particles move to the stagnation plane from $-\infty$, and the oxidizer enters just from the opposite. Figure 1 illustrates the investigated configuration encompassing preheat zone, reaction zone and post-flame zone. The location of the flame with respect to the stagnation plane depends on the streams velocity, fuel concentration, particles size, oxidizer Lewis number, ignition temperature of the fuel, etc.

Model assumptions

Basic assumptions applied to functionalize the model and achieve an analytical solution are presented below:

1. Thermophysical properties of both fuel and oxidizer, such as density, heat capacity and transport coefficients, are assumed to be constant and are presented in Table 1.

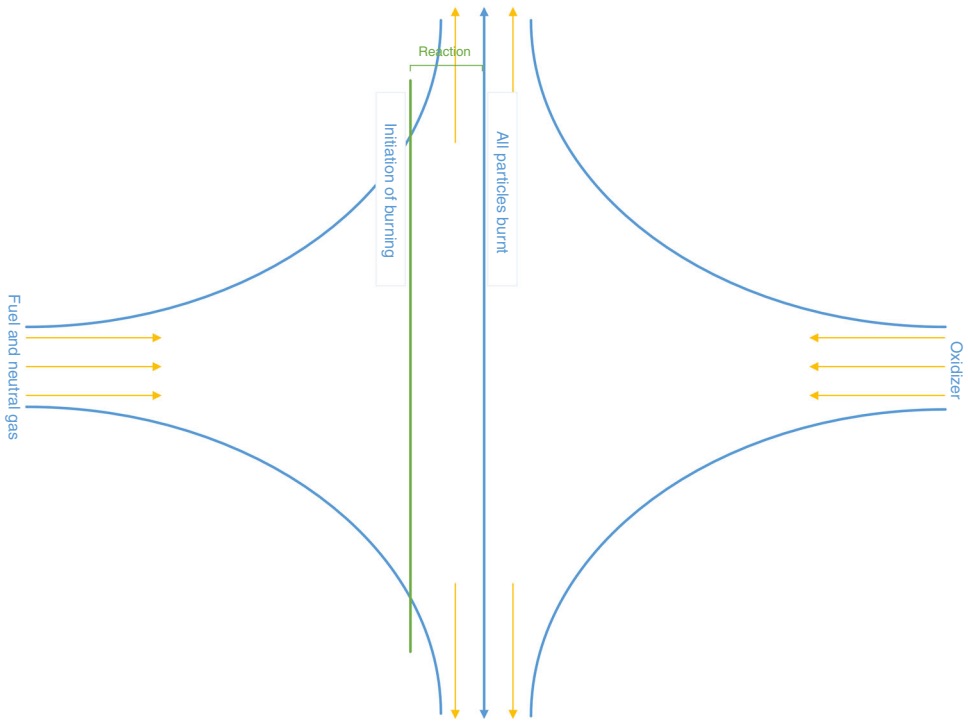

Fig. 1 Schematic of counterflow configuration for the non-premixed flame of aluminum dust cloud and oxidizer

Table 1 Thermophysical properties of air and aluminum used in the model

Air properties	Value	Unit	References
Air properties			
Density	1.164	kg m^{-3}	[36]
Ambient temperature	300	K	[36]
Heat capacity	1.005	kJ kg^{-1} K^{-1}	[36]
Aluminum properties			
Density	2707	kg m^{-3}	[36]
Heat capacity	0.896	kJ kg^{-1} K^{-1}	[36]
Ignition temperature	$T_{ig} = 34.5d_p + 789.1$	K	[37]

2. Aluminum particles enter the combustion domain while being transported by a neutral gas stream with a velocity equal to that of the oxidizer.
3. Heat losses and radiation heat transfer mechanism are neglected [35].
4. The streams are assumed to be laminar and steady.
5. Oxidizer depletion effects are neglected.

Governing equations

Three conservation equations of mass and energy are solved with respect to the defined case study. The velocity field is considered to be as:

$$(u, v) = (-aX, aY) \tag{1}$$

where u and v are velocity in X- and Y-directions and the so-called strain rate, a, represents the velocity gradient at the stagnation plane. Chemical kinetics of reaction is assumed to be as follows:

$$v_S[S] + v_O[O] \rightarrow v_{product}[P] \tag{2}$$

$[S]$, $[O]$ and $[P]$ indicate fuel, oxidizer and product, respectively, and v is the stoichiometric coefficient of reaction. Neglecting the diffusion of solid particles, fuel mass conservation will be in the form of

$$aX\frac{dY_s}{dX} = \frac{\omega_s}{\rho} \tag{3}$$

where Y_s and ρ show particle mass fraction and density, respectively. ω_s is the reaction rate which is defined as [38]

$$\omega_s = Y_s \cdot Y_o \cdot k_0 \cdot \exp\left(-\frac{E_a}{RT}\right) \tag{4}$$

where Y_o, k_0, E_a, R and T are oxidizer mass fraction, pre-exponential factor of the reaction, reaction activation

energy, universal gas constant and temperature, respectively.

$$-aX\frac{\mathrm{d}Y_{\mathrm{O}}}{\mathrm{d}X}=D_{\mathrm{O}}\frac{\mathrm{d}^2Y_{\mathrm{O}}}{\mathrm{d}X^2}-\vartheta\frac{\omega_{\mathrm{s}}}{\rho} \tag{5}$$

Equation 5 represents oxidizer mass conservation in which D_{O} and ϑ are the oxidizer diffusion coefficient and the stoichiometric mass ratio of oxidizer to fuel. Conservation of energy equation is depicted below:

$$-aX\frac{\mathrm{d}T}{\mathrm{d}X}=D_{\mathrm{T}}\frac{\mathrm{d}^2T}{\mathrm{d}X^2}+\omega_{\mathrm{s}}\frac{Q}{\rho C} \tag{6}$$

Here, Q is the heat released per unit mass of fuel during reaction, D_{T} is thermal diffusion coefficient which is equal to $\frac{\lambda}{\rho C}$, and C is the heat capacity of the mixture, calculated from the relation below:

$$C=C_{\mathrm{a}}+\frac{4\pi r^3C_{\mathrm{p}}\rho_{\mathrm{p}}n_{\mathrm{p}}}{3\rho} \tag{7}$$

where the subscripts a and p refer to air and particle, respectively, and n_{p} is the number of particles per unit volume.

Dimensionless form of equations

Some dimensionless parameters are used to unravel the equations and gain a more comprehensive knowledge of certain combustion characteristics. The parameters θ, y_{S}, y_{o} and x are the dimensionless forms of temperature, fuel and oxidizer mass fraction and length, respectively.

$$\theta=\frac{C(T-T_\infty)}{QY_{\mathrm{S}-\infty}},\quad y_{\mathrm{S}}=\frac{Y_{\mathrm{S}}}{Y_{\mathrm{S}-\infty}},\quad y_{\mathrm{o}}=\frac{Y_{\mathrm{O}}}{\vartheta Y_{\mathrm{s}-\infty}},\quad x=\frac{X}{\sqrt{\frac{\lambda}{\rho Ca}}} \tag{8}$$

where $Y_{\mathrm{S}-\infty}$ is the initial mass fraction of the fuel. It is required here to mention the so-called dimensionless Lewis number, which represents the ratio of conduction to diffusion. In this study, the Lewis number is assumed to be of non-unit and its effects on the flame are investigated thoroughly.

$$Le=\frac{\lambda}{\rho CD} \tag{9}$$

Substituting the above parameters and reaction rate in Eq. 4 to Eqs. 3, 5, 6 and performing algebraic operations, general dimensionless conservation equations of fuel and oxidizer mass fractions and energy yield:

$$x\frac{\mathrm{d}y_{\mathrm{s}}}{\mathrm{d}x}=D_{\mathrm{c}}\cdot y_{\mathrm{s}}\cdot y_{\mathrm{o}}\cdot\exp\left(-\frac{T_{\mathrm{a}}}{T}\right) \tag{10}$$

$$x\frac{\mathrm{d}y_{\mathrm{O}}}{\mathrm{d}x}+\frac{1}{Le_{\mathrm{O}}}\frac{\mathrm{d}^2y_{\mathrm{O}}}{\mathrm{d}x^2}=D_{\mathrm{c}}\cdot y_{\mathrm{s}}\cdot y_{\mathrm{o}}\cdot\exp\left(-\frac{T_{\mathrm{a}}}{T}\right) \tag{11}$$

$$\frac{\mathrm{d}^2\theta}{\mathrm{d}x^2}+x\frac{\mathrm{d}\theta}{\mathrm{d}x}=-D_{\mathrm{c}}\cdot y_{\mathrm{s}}\cdot y_{\mathrm{o}}\cdot\exp\left(-\frac{T_{\mathrm{a}}}{T}\right) \tag{12}$$

Le_{O} is the oxidizer Lewis number, T_{a} shows dimensionless activation energy which is equal to $\frac{E}{R}$, and D_{c} is defined as below:

$$D_{\mathrm{C}}=k_0\vartheta_{\mathrm{O}}Y_{\mathrm{S}-\infty}/W_{\mathrm{F}}a \tag{13}$$

ϑ_{O} is the number of moles of oxygen participating in the reaction with one mole fuel, and W_{F} is the molecular weight of fuel.

Boundary conditions

As it was mentioned before, the combustion domain is divided into three separate zones each of which has its own form of conservation equations and boundary conditions. The three zones are defined as:

Preheat zone: $Z_1:-\infty<x\leq x_{\mathrm{f}}$
Reaction zone: $Z_2:x_{\mathrm{f}}\leq x\leq 0$
Post-flame zone: $Z_3:0\leq x\leq+\infty$

x_{f} shows the location in which reaction begins. Assuming the above divisions, boundary conditions will be as follows:

$$x\to-\infty\quad y_{\mathrm{s}}=1\quad y_{\mathrm{O}}=0\quad\theta=0 \tag{14}$$

$$x=x_{\mathrm{f}}\quad y_{\mathrm{s}}=1\quad y_{\mathrm{O}}=0\quad\theta=\theta_{\mathrm{ig}} \tag{15}$$

$$x=0\quad y_{\mathrm{s}}=0\quad y_{\mathrm{O}}=1\quad\theta=\theta_0 \tag{16}$$

$$x\to+\infty\quad y_{\mathrm{s}}=0\quad y_{\mathrm{O}}=1\quad\theta=0 \tag{17}$$

$\theta=0$, θ_{ig}, θ_0 correspond to ambient temperature, temperature required for the particles to start to burn and the temperature in the stagnation plane calculated from the preheat zone.

Solution

- $Z_1:-\infty<x\leq x_{\mathrm{f}}$

This zone consists of particles exiting the fuel nozzle and being preheated until they reach the reaction zone. As the fuel temperature is under its ignition temperature, no reaction occurs and, therefore, reaction term is deleted from Eqs. 10, 11 and 12. According to Eqs. 14 and 15, the conservation equations for this zone are solved as below:

$$y_s = 1 \tag{18}$$

$$y_O = 0 \tag{19}$$

$$\theta = \left[\frac{\theta_{ig}}{\operatorname{erfc}\left(\frac{-x_f}{2}\right)}\right]\operatorname{erfc}\left(\frac{-x}{2}\right) \tag{20}$$

- $Z_3 : 0 \le x \le +\infty$

This area includes the entry point of the oxidizer to the combustion domain. Considering the fuels to be fully burnt in this zone, no reaction occurs here, too. So the conservation equations are acquired by the similar approach to that of the Z_1, which are given below:

$$y_s = 0 \tag{21}$$

$$y_O = 1 \tag{22}$$

$$\theta = \theta_0 \cdot \operatorname{erfc}\left(\frac{x}{2}\right) \tag{23}$$

- $Z_2 : x_f \le x \le 0$

In this region, the particles have reached the ignition temperature and burn heterogeneously and the three conservation equations for this zone are exactly the same as Eqs. 10, 11 and 12. We have three coupled nonlinear differential equations with four variables of y_o, y_S, T and x_f, for which no certain analytical solution is available. For the purpose of solving the system, the position of x_f should be known which can be calculated from the jump condition below. By performing algebraic operations on Eqs. 10 and 12, the following relation will be obtained:

$$\frac{d^2\theta}{dx^2} + x\frac{d\theta}{dx} = -x\frac{dy_s}{dx} \tag{24}$$

By numerically integrating the above equation on $\left[x_f^-, x_f^+\right]$, initiation point of reaction will be known as a function of dimensionless temperature and fuel mass fraction. Consequently, a system of nonlinear differential equations consisting of four equations and four unknowns is achieved and solved by an iterative numerical method. Solving the conservation equations for all three zones, flame location and species mass fractions as well as temperature distribution of the mixture are obtained for the entire domain, which enables us to investigate the effect of thermophoretic force as well as other forces exerted on a single metal particle undergoing combustion in a non-premixed counterflow configuration.

Particle motion analysis

The forces exerted on a single metal particle during non-premixed counterflow combustion are studied one by one, and Lagrangian equations of motion are utilized to predict particles path as well as thermophoretic force impact on the system. Calculating the velocity difference between the gas and the particle and differentiation of the temperature distribution achieved before, the path and velocity of a single particle are gained analytically.

- Weight and buoyancy

The integration of gravity and buoyancy forces yields the following relation:

$$F_G + F_B = -\frac{4}{3}\pi r_p^3(\rho_p - \rho_g)g \tag{25}$$

where ρ_p and ρ_g are densities of particle and air, respectively. There are two extreme cases in the nature of the particle and gas interactions, and the Knudsen number is the best measure for the proper formulation to be considered. This number represents the ratio of the molecular mean free path to the physical length scale. When this number is equal to or larger than one, a free molecular regime should be considered; otherwise, a continuum regime will govern the problem. The Knudsen number is defined as:

$$Kn = \frac{2\lambda}{d_p} \tag{26}$$

in which d_p and λ are the particle diameter and mean free path. λ is formulated as

$$\lambda = \mu/(\phi\rho_g\bar{c}) \tag{27}$$

where μ is the viscosity of the gas and $\bar{c}$ as the mean thermal velocity of gaseous molecules is defined as below:

$$\bar{c} = \left(\frac{8RT}{\pi M}\right)^{0.5} \tag{28}$$

Based on the model presented by Allen and Raabe [39], ϕ is equal to 0.491.

- Thermophoretic

A temperature gradient can exert forces on the particles and make them diffuse. This phenomenon is called thermophoresis and is equal to Suret effect in gas compounds. Talbot et al. [40] have developed this relation for thermophoretic force affecting a particle.

$$F_T = -3\pi\mu d_p \vartheta K_T \frac{\nabla T}{T_u} \tag{29}$$

$$K_T = \frac{2C_s\left(\frac{k_g}{k_p} + C_T * Kn\right)}{(1 + 3C_m * Kn)\left(1 + 2\frac{k_g}{k_p} + 2C_t * Kn\right)} \tag{30}$$

where ∇T, T_u, ϑ, k_p, k_g, C_t, C_s and C_m are temperature gradient, ambient temperature, mixture kinematic

viscosity, metal thermal conductivity, air thermal conductivity, thermal creep coefficient, thermal jump coefficient and velocity jump coefficient, respectively. Batchelor and Shen [41] have suggested these values for the three coefficients.

$$C_t = 2.2; \quad C_s = 1.147; \quad C_m = 1.146$$

As the Knudsen number for this specific problem is less than 0.2, continuum regime is a more realistic assumption, so the following relation is employed to calculate thermophoretic force.

$$F_{T,\text{continuum}} = -6\pi\mu^2 d_p \frac{C_s k_g}{k_p + 2k_g} \frac{\nabla T}{\rho_g T_u} \tag{31}$$

- Drag

Drag force acts on the interface between the fluid and the particle. When the particle moves inside the gas, an interaction occurs between them. Shear stress is exerted on the particle due to the effects of viscosity and vertical stress triggered by the pressure gradient. Given the Stokes flow assumptions which relate to small particles with the least slip speed compared to the carrier gas, we have:

$$F_D = \frac{\pi}{8} d_p^2 C_D \rho_g U^2, C_D = \frac{24}{Re} \tag{32}$$

Therefore, the final equation for the drag force can be calculated as follows:

$$F_D = -3\pi\mu d_p U \tag{33}$$

where U is the particle velocity and Re is the Reynolds number.

Lagrangian equation of metal particle motion

Particles are considered to be scattered before they enter the combustion domain, and no collision takes place between them at the entrance. The spherical particle is assumed to be flowing through an inert gas with constant density toward the preheating zone. The particle initially has the same velocity as the carrying gas, but density difference influences particle's path over time. In the x-direction, drag and thermophoretic forces are exerted on the particle, while in the y-direction, there is no temperature gradient, and therefore, the only forces that have an impact on the particle are drag, weight and buoyancy. In Lagrangian method, the curves of motion of each particle are obtained by integrating the following equations:

$$U_x = \frac{dx_p}{dt}, \quad m_p \frac{dU_x}{dt} = F_{D_x} + F_T \tag{34}$$

$$U_y = \frac{dy_p}{dt}, \quad m_p \frac{dU_y}{dt} = F_{D_y} + F_G + F_B \tag{35}$$

Substituting Eqs. 25, 31 and 33 in the above equations and replacing $\frac{dU}{dt}$ with $U\frac{dU}{dx}$, the general equations for the forces in x- and y-directions are obtained as follows:

$$m_p \cdot U \frac{dU}{dx} = -3\pi\mu d_p U - 6\pi\mu^2 d_p \frac{C_s k_g}{k_p + 2k_g} \frac{\nabla T}{\rho_g T_u} \tag{36}$$

$$m_p \cdot U \frac{dU}{dy} = -3\pi\mu d_p U - \frac{1}{6}\pi d_p^3 (\rho_p - \rho_g) g \tag{37}$$

The temperature gradient in Eq. 36 is calculated by numerical differentiation of temperature distribution obtained from Sect. 2.5. Solving the above equations analytically, these two relations are achieved for the velocity in x- and y-directions.

$$U_x = -\frac{\left(\frac{-6\pi\mu^2 d_p C_s k_g}{m_p(k_p+2k_g)} \frac{\nabla T}{\rho_g T_u}\right)\left\{1 + \text{Lambert}\left[-\frac{e^{-1-\frac{\left(-\frac{3\pi\mu d_p}{m_p}\right)^2}{\frac{-6\pi\mu^2 d_p C_s k_g}{m_p(k_p+2k_g)} \frac{\nabla T}{\rho_g T_u}}(x)}}{\frac{-6\pi\mu^2 d_p C_s k_g}{m_p(k_p+2k_g)} \frac{\nabla T}{\rho_g T_u}}\right]\right\}}{-\frac{3\pi\mu d_p}{m_p}} \tag{38}$$

$$U_y = -\frac{\left(\frac{-\pi\mu d_p^3 g(\rho_p-\rho_g)}{6m_p}\right)\left\{1 + \text{Lambert}\left[-\frac{e^{-1-\frac{\left(-\frac{3\pi\mu d_p}{m_p}\right)^2}{\frac{-\pi\mu d_p^3 g(\rho_p-\rho_g)}{6m_p}}(y)}}{\frac{-\pi\mu d_p^3 g(\rho_p-\rho_g)}{6m_p}}\right]\right\}}{-\frac{3\pi\mu d_p}{m_p}} \tag{39}$$

Finally, by integrating Eqs. 38 and 39 on the combustion domain, particle path in the 2D coordinates is calculated numerically.

Results

The metal fuel used to investigate the non-premixed counterflow combustion is aluminum particles with the diameter of 5.4 μm, and the quantities of the parameters employed in the conservation equations are extracted from the studies [20, 38]. Besides, the inert gas flow carrying aluminum particles are assumed to be nitrogen. Thermal properties of air and aluminum particles are assumed to be constant and are presented in Table 1.

To obtain the exact initiation point of reaction, the ignition temperature of aluminum is extracted from the results of Marino's study [37]. He has correlated and reported a relation for the ignition temperature of

aluminum particles in terms of diameter which is depicted below.

$$T_{ig} = 34.5d_p + 789.1 \tag{40}$$

The reaction that occurs during the combustion process is as follows:

$$4Al + 3(O_2 + 3.76N_2) \rightarrow 2Al_2O_3 + 11.28N_2 \tag{41}$$

$Y_{S-\infty}$ is calculated in terms of number and diameter of the particles as follows:

$$Y_{S-\infty} = \frac{\frac{4}{3}\pi r_p^3 n_p \rho_p}{\rho} \tag{42}$$

Another definition used to report data is the mass concentration of the fuel which is defined as

$$C_m = \frac{4}{3}\pi r_p^3 n_p \rho_p \tag{43}$$

Figure 2 presents the flame temperature in terms of oxidizer Lewis number for three different fuel mass concentrations. Lewis number represents the ratio of heat to mass diffusion; therefore, an increase in oxidizer Lewis number causes the deficiency in the oxidizer supply to the flame and reduces the flame temperature. For example, a change in oxidizer Lewis number of 0.6–1.4 lowers the temperature from 2927 to 2485 K. Furthermore, as expected, increasing the amount of fuel (concentration) leads to higher flame temperatures. For oxidizer Lewis number equal to one, with 400 g m^{-3} increase in the mass concentration of the fuel, the flame temperature increases by 63%.

The impact of oxidizer Lewis number on the flame initiation position for different fuel mass concentrations is depicted in Fig. 3. As it is shown, the increase in oxidizer Lewis number causes more thermal diffusivity compared to mass diffusivity and, therefore, the amount of oxidizer reaching the flame decreases, leading to a flame nearer to the oxidizer nozzle. It can be observed that by increasing the fuel concentration, the flame goes away from fuel nozzle which is due to the increase in the heat required for fuel to reach its ignition temperature.

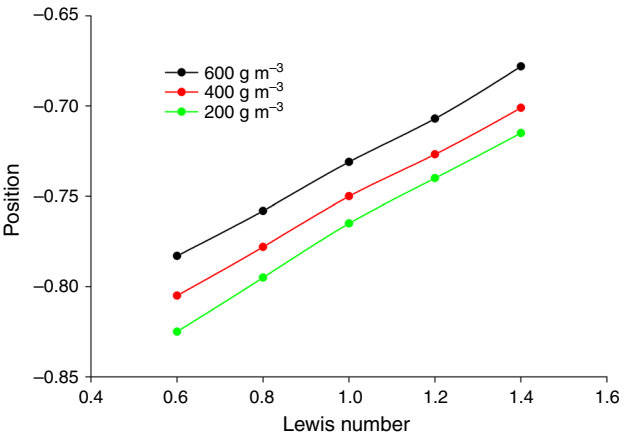

Fig. 3 Flame position versus oxidizer Lewis number for different fuel mass concentrations

Figure 4 indicates the temperature profile of the mixture through the whole domain for three different concentrations of the fuel and oxidizer Lewis number of 1. As shown in the figure, the fuel and oxidizer temperatures, in the left and right sides of stagnation plane, respectively, gradually increase to reach the maximum flame temperature at $x = 0$. By the time that particle flares, due to the assumption of Arrhenius model for the reaction and the presence of an exponential term, the increase in temperature is accompanied by a delay until particles reach the end of the reaction region at $x = 0$, and then returns to the ambient temperature. As can be seen in the figure, an increase in the concentration of the fuel leads to an increase in the maximum temperature of the mixture, because of the more fuel available for combustion, causing the initiation point of

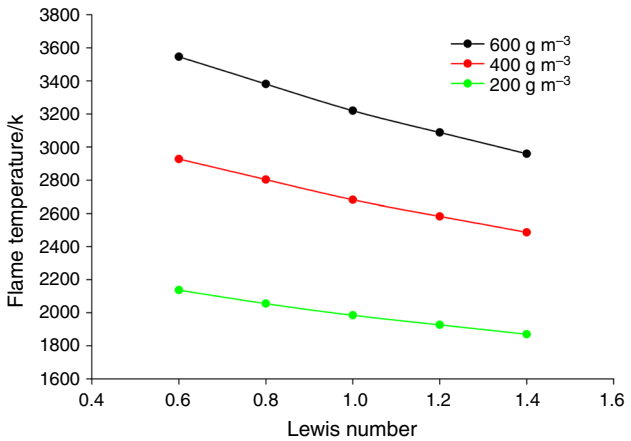

Fig. 2 Flame temperature versus oxidizer Lewis number for different fuel mass concentrations

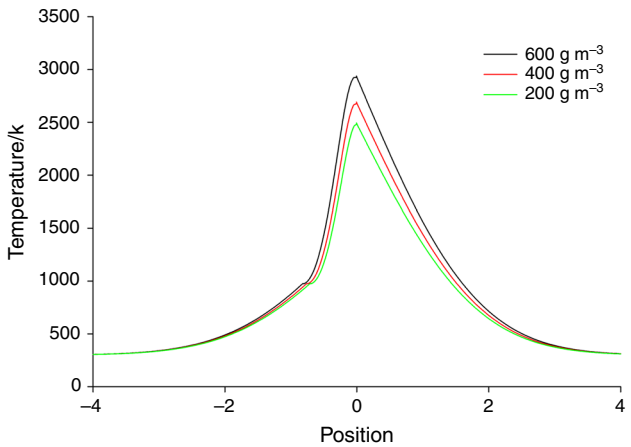

Fig. 4 Temperature profiles through the entire domain of combustion for three different fuel mass concentrations

reaction approaching the oxidizer nozzle. Maximum flame temperature for concentrations 200, 400 and 600 g m^{-3} is 2481, 2677 and 2927 K, respectively. As it was mentioned, the ignition temperature of 5.4-μm aluminum particles is calculated to be 975 K using Eq. 40.

Figure 5 outlines the path of aluminum particles with different diameters and the carrier inert gas. As it was mentioned before, particle enters the preheat zone with the same velocity as the gas flow from the fuel nozzle at the left side of the domain, but due to their density difference over time, the path and velocity of the particle will vary from that of the carrier gas. The black curve represents the direction of carrier gas which is extracted from Eq. 1, and the other curves indicate the deviation of particles paths of each size aroused by the forces exerted on particles including weight, buoyancy, drag and thermophoretic forces. It is clear that by an increase in the particle diameter, a greater deviation occurs to the extent that particles enter the oxidizer zone after being burnt, which is due to the greater inertia of particles.

Figure 6 indicates the effect of thermophoresis on a 5.4-μm aluminum particle's path undergoing the non-premixed counterflow combustion. As can be seen, considering the related thermophoresis term in the forces balance equation leads to a direction less deviated from the inert gas flow. It is because of the fact that mixture molecules nearer to the stagnation plane own higher temperatures and therefore higher kinetic energy, colliding more with the fuel particles and pushing them down the temperature gradient.

Model validation

The inability to control the flame in non-premixed counterflow combustion and the difficulties that arise in maintaining safety issues are the main reasons why few experimental studies have been conducted on the diffusion flames, especially with the solid fuel particles. For the first time, Julien et al. [42] investigated the laminar diffusion flame of aluminum dust cloud in counterflow configuration and measured the burning velocity in terms of fuel concentration. They compared the results obtained from their experiments with previous data for stabilized flames, spherically expanding flames and flames propagating in tubes. In this study, in order to validate the proposed model, the results of Julien's study are used, the comparison of which is shown in Fig. 7. The average particle diameter in the test is 6 μm, and the diameter of the particles in the present model is considered to be 5.4 μm. In order to verify the accuracy of the model, the burning velocity of the particles was compared with the results of study mentioned. In non-premixed counterflow combustion, the flame forms where there is a balance between the burning velocity and the local flow velocity; therefore, it is determined by the relation $V_b = a * x$. It is obvious that the

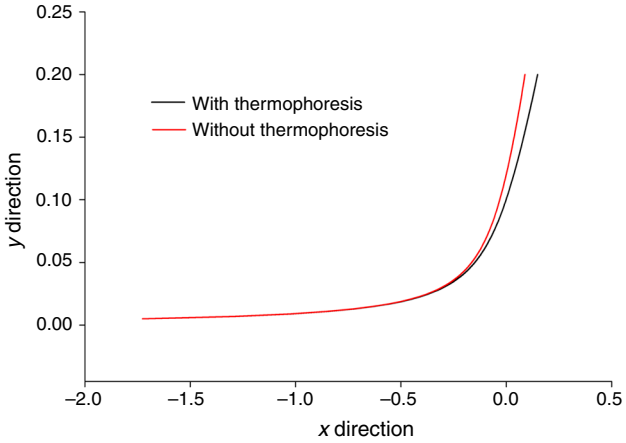

Fig. 6 A single 5.4-μm aluminum particle's path with and without considering the thermophoretic force

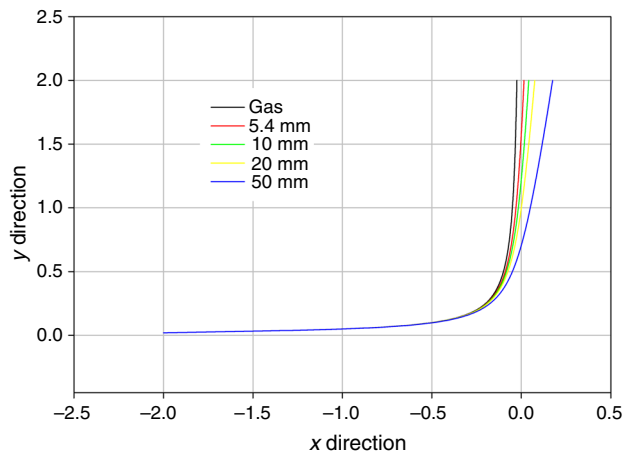

Fig. 5 Paths of the gas flow and particles with different diameters

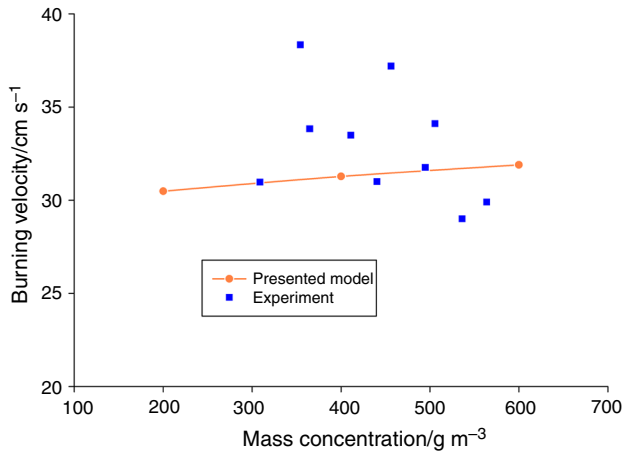

Fig. 7 Comparison of the burning velocity for the presented model with the results of Julien et al. [42]

model is able to predict the burning velocities with good approximation given the uncertainties of the numerical solution and simplifying assumptions. Julien et al. acclaimed the independency of the burning velocity on the mass concentration which is clearly repeated by the model.

Conclusions

A semi-mathematical model is developed for non-premixed combustion of metal dusts in counterflow configuration. This is done by solving the energy and mass conservation equations for each zone including preheat, reaction and oxidizer zones which are defined based on corresponding boundary and jump conditions. The model indicates that increasing fuel mass concentration by 200% or decreasing oxidizer Lewis number by 57% will result in a 36% and 12% increase in flame temperature, respectively. It also calculates the temperature distribution of combustion domain and examines the effects of fuel mass concentration and oxidizer Lewis number on the location of the flame. In case of particle tracking, 2D Lagrangian equations of motion are derived based on various forces exerted on a single particle and its path and velocity are achieved with respect to the carrier neutral gas. The results showed that the thermophoretic force affects the particle motion path by 3% and should not be neglected for this particular velocity field and temperature distribution. Furthermore, the model is satisfactorily successful in predicting the combustion characteristics, which are consistent with the experimental data available in the literature, and the partial disputes are justifiable by the simplistic assumptions of the model. Additionally, this model not only gives an insight into the aluminum particle cloud, but also is applicable for any metal dust acting as fuel in counterflow configuration.

References

1. Matveeva EG, Gryczynski Z, Lakowicz JR. Myoglobin immunoassay based on metal particle-enhanced fluorescence. J Immunol Methods. 2005;302:26–35.
2. Lee YK, Kim J, Kim Y, Kwak JW, Yoon Y, Rogers JA. Room temperature electrochemical sintering of Zn microparticles and its use in printable conducting inks for bioresorbable electronics. Adv Mater. 2017;29:1702665.
3. Hemmat Esfe M, Saedodin S, Bahiraei M, Toghraie D, Mahian O, Wongwises S. Thermal conductivity modeling of MgO/EG nanofluids using experimental data and artificial neural network. J Therm Anal Calorim. 2014;118:287–94.
4. Sarafraz M, Nikkhah V, Madani SA, Jafatian M, Hormozi F. Low-frequency vibration for fouling mitigation and intensification of thermal performance of a plate heat exchanger working with CuO/water nanofluid. Appl Therm Eng. 2017;121:388–99.
5. Toghraie D, Chaharsoghi VA, Afrand M. Measurement of thermal conductivity of ZnO–TiO_2/EG hybrid nanofluid. J Therm Anal Calorim. 2016;125:527–35.
6. Zadkhast M, Toghraie D, Karimipour A. Developing a new correlation to estimate the thermal conductivity of MWCNT–CuO/water hybrid nanofluid via an experimental investigation. J Therm Anal Calorim. 2017;129:859–67.
7. Toghraie D, Abdollah MMD, Pourfattah F, Akbari OA, Ruhani B. Numerical investigation of flow and heat transfer characteristics in smooth, sinusoidal and zigzag-shaped microchannel with and without nanofluid. J Therm Anal Calorim. 2018;131:1757–66.
8. Hemmat Esfe M, Ahangar MRH, Toghraie D, Hajmohammad MH, Rostamian H, Tourang H. Designing artificial neural network on thermal conductivity of Al_2O_3–water–EG (60–40%) nanofluid using experimental data. J Therm Anal Calorim. 2016;126:837–43.
9. Pandas HM, Fazli M. Fabrication of MgO and ZnO nanoparticles by the aid of eggshell bioactive membrane and exploring their catalytic activities on thermal decomposition of ammonium perchlorate. J Therm Anal Calorim. 2018;131:2913–24.
10. Dumitru R, Manea F, Lupa L, Păcurariu C, Lanculecsa A, Baciu A, Negria S. Synthesis, characterization of nanosized $CoAl_2O_4$ and its electrocatalytic activity for enhanced sensing application. J Therm Anal Calorim. 2017;128:1305–12.
11. Arya A, Sarafraz MM, Shahmiri S, Madani SAH, Nikkhah V, Nakhjavani SM. Thermal performance analysis of a flat heat pipe working with carbon nanotube-water nanofluid for cooling of a high heat flux heater. Heat Mass Transf. 2018;54:985–97.
12. Subramani J, Nagarajan PK, Mahian O, Sathyamurthy R. Efficiency and heat transfer improvements in a parabolic trough solar collector using TiO_2 nanofluids under turbulent flow regime. Renew Energy. 2018;119:19–31.
13. Bergthorson J, Goroshin S, Soo M, Julien P. Direct combustion of recyclable metal fuels for zero-carbon heat and power. Appl Energy. 2015;160:368–82.
14. Li G, Yang H, Yuan C, Eckhoff R. A catastrophic aluminium-alloy dust explosion in China. J Loss Prev. 2016;39:121–30.
15. Li Q, Wang K, Zheng Y, Mei X, Lin B. Explosion severity of micro-sized aluminum dust and its flame propagation properties in 20 L spherical vessel. Powder Technol. 2016;301:1299–308.
16. Abbasi T, Abbasi SA. Dust explosions–cases, causes, consequences, and control. J Hazard Mater. 2007;140:7–44.
17. Dreizin EL, Trunov MA. Surface phenomena in aluminum combustion. Combust Flame. 1995;101:378–82.
18. Tang F-D. Reaction-diffusion fronts in heterogeneous combustion. Montreal: McGill University; 2011.
19. Goroshin S, Higgins A, Kamel M. Powdered metals as fuel for hypersonic ramjets. In: 37th joint propulsion conference and exhibit. Reston, Virigina: American Institute of Aeronautics and Astronautics; 2001.
20. Beckstead MW. A summary of aluminum combustion. Provo: Brigham Young University; 2004.
21. Goroshin S, Fomenko I, Lee J. Burning velocities in fuel-rich aluminum dust clouds. Symp Combust. 1996;26:1961–7.
22. Trunov M, Schoenitz M, Dreizin E. Ignition of aluminum powders under different experimental conditions. Propellants Explos Pyrotech. 2005;30:36–43.
23. Risha GA, Huang Y, Yetter RA, Yang V. Experimental investigation of aluminum particle dust cloud combustion. In: Proceedings of 43rd aerospace science meeting and exhibit, Reno, Nevada; 2005.
24. Huang Y, Risha GA, Yang V, Yetter RA. Effect of particle size on combustion of aluminum particle dust in air. Combust Flame. 2009;156:5–13.

25. Bidabadi M, Biouki SA, Afzalabadi A, Dehghan AA, Poorfar AK, Rouboa A. Modeling propagation and extinction of aluminum dust particles in a reaction medium with spatially uniform distribution of particles. J Therm Anal Calorim. 2017;129:1855–64.
26. Bidabadi M, Mohebbi M, Poorfar A. Modeling quenching distance and flame propagation speed through an iron dust cloud with spatially random distribution of particles. J Loss Prev Process Ind. 2016;43:138–46.
27. Afzalabadi A, Poorfar AK, Bidabadi M, Moghadasi H, Hochgreb S, Rahbari A, et al. Study on hybrid combustion of aero-suspensions of boron-aluminum powders in a quiescent reaction medium. J Loss Prev Process Ind. 2017;49:645–51.
28. Bidabadi M, Zadsirjan S, Mostafavi SA. Radiation heat transfer in transient dust cloud flame propagation. J Loss Prev Process Ind. 2013;26:862–8.
29. Seshadri K, Trevino C. The influence of the Lewis numbers of the reactants on the asymptotic structure of counterflow and stagnant diffusion flames. Combust Sci Technol. 1989;64:243–61.
30. Guo H, Ju Y, Maruta K, Niioka T, Liu F. Radiation extinction limit of counterflow premixed lean methane-air flames. Combust Flame. 1997;109:639–46.
31. Seiser R, Pitsch H, Seshadri K, Pitz WJ, Gurran HJ. Extinction and autoignition of n-heptane in counterflow configuration. Proc Combust Inst. 2000;28:2029–37.
32. Bidabadi M, Akbari Vakilabadi M, Khoeini Poorfar A, Monteiro E, Rouboa A, Rahbari A. Mathematical modeling of premixed counterflow combustion of organic dust cloud. Renew Energy. 2016;92:376–84.
33. Mohammadi M, Bidabadi M, Khalili H. Modeling counterflow combustion of dust particle cloud in heterogeneous media. J Energy Eng. 2016. https://doi.org/10.1061/(ASCE)EY.1943-7897.0000394.
34. Bidabadi M, Ramezanpour M, Mohammadi M, Fereidooni J. The effect of thermophoresis on flame propagation in nano-aluminum and water mixtures. Period Polytech Chem Eng. 2016;60(3):157–64.
35. Bidabadi M. An experimental and analytical study of laminar dust flame propagation. Doctoral dissertation. McGill University; 1995.
36. Bergman TL, Incropera FP. Fundamentals of heat and mass transfer. London: Wiley; 2011.
37. Marino T. Numerical analysis to study the effects of solid fuel particle characteristics on ignition, burning, and radiative emission. Doctoral dissertation. The George Washington University; 2008.
38. Law CK. Combustion physics. Cambridge: Cambridge University Press; 2010.
39. Allen MD, Raabe OG. Re-evaluation of Millikan's oil drop data for the motion of small particles in air. J Aerosol Sci. 1982;13:537–47.
40. Talbot L, Cheng RK, Schefer RW, Willis DR. Thermophoresis of particles in a heated boundary layer. J Fluid Mech. 1980;101:737–58.
41. Batchelor GK, Shen C. Thermophoretic deposition of particles in gas flowing over cold surfaces. J Colloid Interface Sci. 1985;107:21–37.
42. Julien P, Whiteley S, Soo M, Goroshin S. Flame speed measurements in aluminum suspensions using a counterflow burner. Proc Combust Inst. 2017;36:2291–8.